

Ultra-High Energy Cosmic Ray production in the polar cap regions of black hole magnetospheres.

A.Yu. Neronov^{a,b} D.V. Semikoz^{c,d,e} I.I. Tkachev^e

^a*INTEGRAL Science Data Centre, CH. d'Ecogia 16, Verosox, 1290, Switzerland*

^b*Geneva Observatory, Ch. des Maillettes, Versoix 1290, Switzerland*

^c*APC, 10, rue Alice Domon et Leonie Duquet, F-75205 Paris Cedex 13, France*

^d*CERN Theory Division, CH-1211 Geneva 23, Switzerland*

^e*Institute for Nuclear Researches of the Russian Academy of Sciences, 60th October Anniversary Prosp. 7a, 117312, Moscow, Russia*

Abstract

We develop a model of ultra-high energy cosmic ray (UHECR) production via acceleration in a rotation-induced electric field in vacuum gaps in the magnetospheres of supermassive black holes (BH). We show that if the poloidal magnetic field near the BH horizon is misaligned with the BH rotation axis, charged particles, which initially spiral into the BH hole along the equatorial plane, penetrate into the regions above the BH "polar caps" and are ejected with high energies to infinity. We show that in such a model acceleration of protons near a BH of typical mass 3×10^8 solar masses is possible only if the magnetic field is almost aligned with the BH rotation axis. We find that the power of anisotropic electromagnetic emission from an UHECR source near a supermassive BH should be at least 10-100 times larger than UHECR power of the source. This implies that if the number of UHECR sources within the 100 Mpc sphere is ~ 100 , the power of electromagnetic emission which accompanies proton acceleration in each source, 10^{42-43} erg/s, is comparable to the typical luminosities of active galactic nuclei (AGN) in the local Universe. We also explore the acceleration of heavy nuclei, for which the constraints on the electromagnetic luminosity and on the alignment of magnetic field in the gap are relaxed.

1 Introduction

Recent observations of fast-variability of the very-high-energy (VHE) γ -ray emission from a nearby radio-galaxy M87 [1] and from several blazars, Mkn

501 [2], PKS 2155-304 [3] show that the central engines of active galactic nuclei (AGN), the supermassive black holes (BHs), most probably operate as powerful particle accelerators. The observed variability time scales, which are of the order of, or shorter than the light crossing times of the BH horizons, put tight constraints on the possible locations of particle accelerators in these objects.

The compactness of the accelerators operating in the vicinity of the supermassive BHs (the characteristic size scale is set up by the Schwarzschild radius, $R_{\text{Schw}} = 2GM \simeq 3 \times 10^{13} [M/10^8 M_{\odot}]$ cm, where M is the BH mass and G is the Newton's constant) makes particle acceleration in these objects difficult, because of the inevitably strong energy losses related to the synchrotron/curvature radiation of the accelerated particles (see e.g. [4,5,6]). The fact that, in spite of the strong energy loss rate, these accelerators produce electrons with energies of at least 10-100 TeV (the spectrum of the radio galaxy M87 extends at least up to 20 TeV without a signature of a cut-off), implies that the mechanism of acceleration operating in these objects is highly efficient [7]. An obvious candidate for such a highly efficient (i.e. fast) acceleration mechanism is acceleration of charged particles in a strong large scale electric field, which can be induced in the BH magnetosphere e.g. via the rotational drag of the magnetic field by the black hole, or in the regions of magnetic field reconnection in the accretion disk.

Large scale ordered electric fields, induced by rotation of the compact object, are known to be responsible for particle acceleration and high-energy radiation in pulsars (see e.g. [8]). In the case of pulsars, it is known that particles are accelerated in the so-called "vacuum gaps" in magnetosphere, in which the rotation-induced electric field is not neutralized by redistribution of charges. A similar mechanism of generation of large electric fields can be realized in the vicinity of a rotating BH [9,10]. Moreover, it has been argued that vacuum gaps should form also in the vicinity of a rotating BH [11,12,13,14], which means that a mechanism of particle acceleration similar to the one operating in pulsars should work also in the BH-powered sources. The observational consequences of acceleration in the vacuum gaps of BH magnetospheres were studied as a possible mechanism of powering the AGN jet [11,15,16] and neutrino emission [17] from AGN.

Simple order of magnitude estimates show that, in principle, the mechanism of particle acceleration in the vicinity of supermassive BHs can result in production of the ultra-high-energy cosmic rays (UHECR) (see e.g. [18]). At the same time, the existence of the Greisen-Zatsepin-Kuzmin (GZK) cutoff [19,20] in the spectrum of UHECR, found by the HiRes experiment [21] and confirmed recently by Pierre Auger Observatory [22], points to the astrophysical origin of the primary cosmic ray particles. In this case most of the cosmic rays with energies above the cut-off energy $E \simeq 10^{20}$ eV should come from nearby

sources located at the distance $D < 100$ Mpc. Moreover, analysis of the combined HiRes, AGASA, SUGAR and Yakutsk data reveals anisotropy of arrival directions of the highest energy events, which could be related to the local Universe large scale structure [23,24]. Recently Pierre Auger Observatory has found a correlation of the arrival directions of the highest energy events with the sky positions of the nearby AGN [25].

The model of UHECR production in the nuclei of nearby normal and/or active galaxies was considered before (see e.g. [26]). In particular, the possibility of UHECR generation near the supermassive BH in the nuclei of normal galaxies (the so-called dead quasars), was studied in the Refs. [27,4,6]. As it is mentioned above, in this particular case the compactness of the source makes the acceleration to the UHECR energies ($> 10^{20}$ eV) only marginally possible. A numerical study of the limit on the maximal energies attainable by the accelerated protons reported in Ref. [6] has revealed that, in general, acceleration to the energies above 10^{20} eV is possible only in the vicinity of the most massive BHs (with the masses of the order of $10^{10} M_{\odot}$), which are relatively rare. Besides, such acceleration is accompanied by strong electromagnetic emission, with a luminosity about 2-3 orders of magnitude higher than the UHECR luminosity of the source. This implies that the electromagnetic luminosity of each of the UHECR sources should be at the level of $10^{45-46}/N_{\text{source}}$ erg/s, where N_{source} is the number of the nearby UHECR sources (a typical distance to the source $D \sim 50$ Mpc is assumed). If the number of UHECR sources is not very large, such a luminosity is about the luminosity of the quasars. This, apparently, rules out the model of particle acceleration near the supermassive BHs in the nearby normal galaxies (the "dead quasars" [27]) as a possible mechanism of UHECR production in the nearby sources [6].

The results of the Ref. [6] were obtained for the case of acceleration of protons and under the assumption of a general orientation of magnetic field (created by the matter accreting onto the BH) with respect to the rotation axis of the BH.

The assumption of the absence of alignment between the direction of the magnetic field and the black hole rotation axis was justified in the context of the dead quasar model of environment of the supermassive BH. On the contrary, steady AGN activity in the source would result in the production of a stationary accretion disk whose rotation axis is almost aligned with the rotation axis of the BH [28]. Such an alignment would lead to the alignment of the magnetic field with the BH rotation axis. In this paper we investigate (both analytically and numerically) the consequence of alignment of magnetic field with the BH rotation axis for the particle acceleration. We show that if the magnetic field is aligned to within several degrees, production of ultra-high energy protons becomes possible even for BH of moderate mass ($M \sim 10^8 M_{\odot}$), provided that the magnetic field is very strong ($\sim 10^5$ G). We also show that

the constraint on the strength and alignment of the magnetic field is largely relaxed in the case of acceleration of heavy nuclei to the ultra-high energies ($\geq 10^{20}$ eV).

The assumptions of alignment of magnetic field with the BH rotation axis and/or of acceleration of heavy nuclei lead also to a decrease of the estimate of the power of electromagnetic radiation which accompanies the acceleration. In these cases the electromagnetic luminosity of the vacuum gap at least does not exceed the typical luminosities of the AGN in the local Universe.

The plan of the paper is as follows. In Section 2 we discuss the possible location, geometry and physical conditions in the vacuum gaps close to the BH horizon. To make the presentation self-contained, we give the exact expressions for the rotation induced electric field around a BH placed in an external magnetic field inclined with respect to the rotation axis. In Section 3 we discuss the motion of a charged particle in external gravitational and electromagnetic field near the black hole. In Section 4 we present the results of numerical modelling of such motion and find the dependence of the maximal energies of protons accelerated by the rotation-induced electric field on the main geometrical and physical parameters of the vacuum gap. We find that for reasonable assumptions about the BH mass and the strength of magnetic field the acceleration of protons to the UHECR energies is possible only in the case when the magnetic field is almost aligned with the rotation axis of the black hole (it remains to be seen if such alignment can be achieved in Nature). In Section 5 we calculate, analytically and numerically, the electromagnetic luminosity of the gap and find that the alignment of the magnetic field with the rotation axis reduces the γ -ray luminosity of the gap (making the estimate of the electromagnetic power compatible with the estimates of the luminosity of typical AGN in the local Universe). We find that, apart from the boosting of the maximal energies of accelerated particles and reduction of the electromagnetic power, the alignment of the magnetic field with the rotation axis results in reduction of the probability of the onset of pair production inside the gap which would lead to a “discharge” of the gap and neutralization of the large scale electric field. In Section 6 we explore the acceleration of heavy nuclei in the vacuum gaps and show that, contrary to the case of proton acceleration, the energies of nuclei can reach 10^{20} eV already at moderate magnetic field strength and in the absence of alignment of the magnetic field with the rotation axis. Finally, in Section 7 we summarize our results.

2 Vacuum gaps in the BH magnetosphere

Contrary to a neutron star, a BH can not generate its own magnetic field (unless it is charged). However, if the accretion flow onto a BH is magnetized,

a BH is embedded into external magnetic field. Since the structure of the accretion flow varies on the distance scale larger or equal to the size of the BH horizon, the external magnetic field can be assumed to be homogeneous at the horizon distance scale.

It turns out that a rotating BH placed in an external magnetic field generates an electric field of quadrupole topology via a mechanism similar to the mechanism of generation of a quadrupole electric field by a rotating dipole magnetic field in the case of a neutron star. The only difference is that in the case of the black hole the rotation of external magnetic field arises due to a rotational drag of external magnetic field, rather than due to the rotation of the star.

2.1 *Rotation-induced electric field.*

An exact solution of Maxwell equations in the background of Kerr space-time of a rotating BH is known for the case of arbitrary inclination angle of an asymptotically homogeneous magnetic field [9,10]. In this solution, the rotational drag of magnetic field by the BH leads to the generation of a large scale electric field close to the BH horizon. This solution can be a first approximation for description of the structure of electromagnetic field in the vacuum gap in the black hole magnetosphere. It is clear, however, that the presence of charge-separated plasma around the gap will, in general, lead to modification of the electromagnetic field structure.

A rotating BH is described by two parameters: its mass M and the angular momentum per unit mass $a < M$ (we use the system of units in which the Newton's constant G_N and the speed of light c are equal to 1). The geometry of space-time in the vicinity of the horizon is described by the Kerr metric

$$ds^2 = -\alpha^2 dt^2 + g_{ik} (dx^i + \beta^i dt) (dx^k + \beta^k dt) \quad (1)$$

$$\alpha = \frac{\rho\sqrt{\Delta}}{\Sigma}; \quad g_{rr} = \frac{\rho^2}{\Delta}; \quad g_{\theta\theta} = \rho^2; \quad g_{\phi\phi} = \frac{\Sigma^2 \sin^2 \theta}{\rho^2}; \quad (2)$$

$$\beta_\phi = -\frac{2aMr}{\Sigma^2}; \quad \Delta = r^2 + a^2 - 2Mr; \quad (3)$$

$$\Sigma^2 = (r^2 + a^2)^2 - a^2 \Delta \sin^2 \theta; \quad \rho^2 = r^2 + a^2 \cos^2 \theta \quad (4)$$

The horizon is situated at $r_H = M + \sqrt{M^2 - a^2}$.

The solution of the Maxwell equations which corresponds to the asymptotically homogeneous magnetic field inclined at angle χ with respect to the BH rotation axis is given by the electromagnetic tensor [10]

$$\begin{aligned}
F_{tr} &= \frac{aMB_0}{\rho^4\Delta} \left[\cos\chi\Delta(r^2 - a^2\cos^2\theta)(1 + \cos^2\theta) + \right. \\
&\quad \left. \sin\chi r \sin\theta \cos\theta \left\{ (r^3 - 2Mr^2 + ra^2(1 + \sin^2\theta) + 2Ma^2\cos^2\theta) \cos\psi - \right. \right. \\
&\quad \left. \left. a(r^2 - 4Mr + a^2(1 + \sin^2\theta)) \sin\psi \right\} \right] \\
F_{t\theta} &= \frac{aMB_0}{\rho^4} \left[2\cos\chi r \sin\theta \cos\theta(r^2 - a^2) + \right. \\
&\quad \left. \sin\chi(r^2\cos 2\theta + a^2\cos^2\theta)(a\sin\psi - r\cos\psi) \right] \\
F_{t\phi} &= \frac{B_0\sin\chi aM}{\rho^2} \sin\theta \cos\theta(a\cos\psi + r\sin\psi) \\
F_{r\theta} &= -B_0\sin\chi(a\cos\psi + r\sin\psi) - \\
&\quad \frac{B_0\sin\chi a}{\Delta} \left[(Mr - a^2\sin^2\theta) \cos\psi - a(r\sin^2\theta + M\cos^2\theta) \sin\psi \right] \\
F_{r\phi} &= B_0\cos\chi r \sin^2\theta + a\sin^2\theta F_{tr} - \\
&\quad B_0\sin\chi \sin\theta \cos\theta \left[(r - a^2M/\Delta) \cos\psi - a(1 + rM/\Delta) \sin\psi \right] \\
F_{\theta\phi} &= B_0\cos\chi\Delta \sin\theta \cos\theta + \\
&\quad \frac{(r^2 + a^2)}{a} F_{t\theta} + B_0\sin\chi \left[(r^2\sin^2\theta + Mr\cos 2\theta) \cos\psi - \right. \\
&\quad \left. a(r\sin^2\theta + M\cos^2\theta) \sin\psi \right]
\end{aligned} \tag{5}$$

where

$$\psi = \phi + \frac{a}{2\sqrt{M^2 - a^2}} \ln \left[\frac{r - M + \sqrt{M^2 - a^2}}{r - M - \sqrt{M^2 - a^2}} \right]. \tag{6}$$

In order to understand the qualitative features of an electromagnetic field configuration in a curved space-time (like the one of the rotating BH) it is convenient to consider the field geometry in a locally Lorentzian reference frame. In the case of Kerr space-time it is convenient to choose the so-called “locally non-rotating” reference frame (LNRF), spanned by the orthonormal basis vectors [29]

$$\begin{aligned}
e_{\hat{0}} &= \frac{\Sigma}{\rho\sqrt{\Delta}} \frac{\partial}{\partial t} + \frac{2Mar}{\Sigma\rho\sqrt{\Delta}} \frac{\partial}{\partial \phi}; \\
e_{\hat{r}} &= \frac{\sqrt{\Delta}}{\rho} \frac{\partial}{\partial r}; \\
e_{\hat{\theta}} &= \frac{1}{\rho} \frac{\partial}{\partial \theta}; \\
e_{\hat{\phi}} &= \frac{\rho}{\Sigma \sin\theta} \frac{\partial}{\partial \phi}.
\end{aligned} \tag{7}$$

In this reference frame the magnetic and electric field vectors are expressed through the components of the tensor of electromagnetic field $F_{\mu\nu}$, given by Eq. (5), as

$$B^{\hat{r}} = \frac{F_{\theta\phi}}{\Sigma \sin \theta}; \quad B^{\hat{\theta}} = -\frac{\sqrt{\Delta} F_{r\phi}}{\Sigma \sin \theta}; \quad B^{\hat{\phi}} = \frac{\sqrt{\Delta} F_{r\theta}}{\rho^2} \quad (8)$$

$$E^{\hat{r}} = \frac{\Sigma F_{tr} - ar F_{r\phi}/\Sigma}{\rho^2}; \quad E^{\hat{\theta}} = \frac{\Sigma F_{t\theta} - ar F_{\theta\phi}/\Sigma}{\rho^2 \sqrt{\Delta}}; \quad E^{\hat{\phi}} = \frac{F_{t\phi}}{\sqrt{\Delta} \sin \theta} \quad (9)$$

The expressions for electric and magnetic field simplify in the case of a magnetic field aligned with the BH rotation axis, $\chi = 0$. The solution of Maxwell equations for this particular case was initially reported in the Ref. [9]. Fig. 1 shows the geometry of electric and magnetic field lines for $\chi = 0$ in the case of a maximally rotating BH $a = M$. Taking the asymptotic expression for \vec{E}, \vec{B} in the limit $r \rightarrow \infty$ one can find that far away from the horizon the electromagnetic field is

$$\begin{aligned} B^{\hat{r}} &\rightarrow B_0 \cos \theta; \quad B^{\hat{\theta}} \rightarrow -B_0 \sin \theta \\ E^{\hat{r}} &\rightarrow -\frac{B_0 a M (3 \cos^2 \theta - 1)}{r^2}; \quad E^{\hat{\theta}} = O(r^{-4}). \end{aligned} \quad (10)$$

The electric field has a quadrupole geometry, which is clearly visible in Fig 1.

In the regions where electric field has a component along the magnetic field, charged particles can be accelerated. Particles of opposite charge sign are accelerated in opposite directions. The acceleration can be avoided only if a particle resides at a surface at which the electric field is orthogonal to the magnetic field (which can be called the “force-free” surfaces), such as the surfaces shown by thick solid and dashed black lines in Fig. 1. The force-free surfaces separate different acceleration regions (with electric field directed along or oppositely to the magnetic field), shown as white ($\vec{E} \cdot \vec{B} > 0$) and grey ($\vec{E} \cdot \vec{B} < 0$) areas in Figs. 1, 2.

As one can see from Fig. 1, the force-free surfaces serve as “attractors” to the particles of a definite charge sign. In the case of magnetic field aligned with the rotation axis, shown in Fig. 1, the surface attracting the positively charged particles (the equatorial plane surface) does not intersect with the force-free surface attracting negatively charged particles (shown by the thick solid black curve). However, as soon as the inclination angle of the magnetic field becomes non-zero, the two force-free surfaces “reconnect” as it is shown in Fig. 2. At moderate inclination angles of the magnetic field, the reconnection

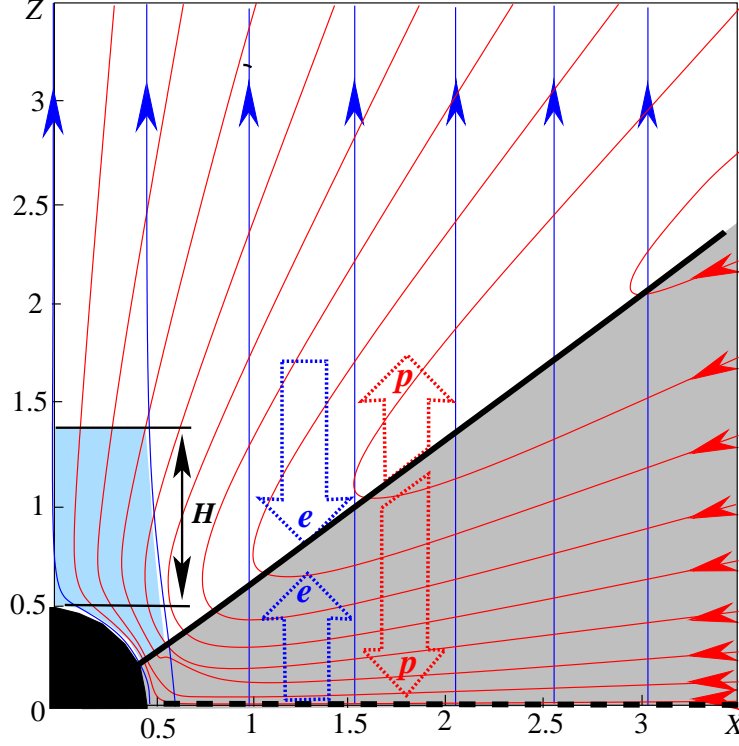


Fig. 1. Magnetic (blue dotted) and electric (red solid) field lines of the field (5) for $a = M$ and $\chi = 0$. The horizon is situated at $r = 0.5(R_{grav}) = M$. Wide blue and red arrows show the directions of acceleration of electrons and protons in different regions. Thick solid and dashed lines show the conical and equatorial “force-free” surfaces. Blue-shaded region shows the location of a vacuum gap into which particles from the equatorial accretion flow can leak if $\chi > 0$.

region is situated close to the equatorial plane, near the BH. The width of the reconnection region grows with the increasing inclination angle. In the following sections we show that charged particles which spiral toward the BH in the equatorial plane, can be accelerated and ejected to infinity when they reach the reconnection region.

2.2 The magnetosphere of rotation-powered black hole

In the presence of an accretion flow the structure of the electromagnetic field around the BH is modified by the redistribution of free charges supplied by the accretion flow. As a result of such redistribution a force-free magnetosphere is formed in which the condition $\vec{B} \perp \vec{E}$ is satisfied. The characteristic charge density needed to neutralize the parallel component of electric field in the magnetosphere of a BH rotating with an angular velocity $\vec{\Omega}$ placed in an

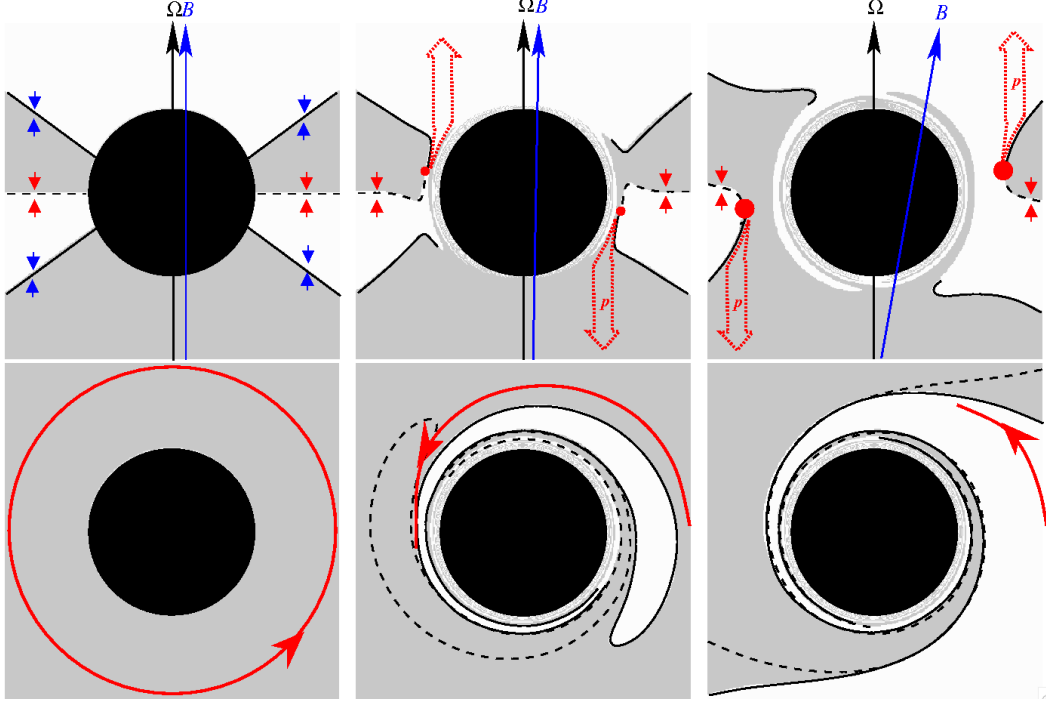


Fig. 2. Evolution of the structure of the force-free surfaces with the increasing misalignment of the magnetic field. The equatorial force-free surface, shown by the dashed line, "reconnects" with the conical force-free surfaces (solid lines) at non-zero inclination angles. Three top panels show the view in the xz plane for the inclination angles $\chi = 0^\circ, \chi = 1^\circ$ and $\chi = 10^\circ$. The bottom panels show the view in the xy plane (just above the equatorial plane, at $z = 0.01R_{\text{Schw}}$) for the same inclination angles. The spiral-like reconnection surfaces, which would be visible if the plane $z = -0.01R_{\text{Schw}}$ would be chosen, are shown by the black dashed curves in the middle and right lower panels. White (grey) areas show the regions where the electric field component along the magnetic field lines has positive (negative) sign. Black circles show the horizon of a maximally rotating BH. Depending on the charge sign, particles in-spiralling toward the BH along the equatorial force-free surface are either ejected to infinity (positively charged particles in this figure, whose typical trajectories are shown by red curves) or are trapped in the region between two force-free surfaces.

external magnetic field \vec{B} is the so-called "Goldreich-Julian" density [30]

$$n_q \simeq \frac{\vec{\Omega} \cdot \vec{B}_{\text{ord}}}{2\pi Ze} \simeq \frac{aB_{\text{ord}}}{Z(GM)^2} \quad (11)$$

In general, the charge distribution in the magnetosphere is not static – additional free charges should be continuously supplied throughout the magnetosphere to compensate for the charge loss due to the magnetohydrodynamical outflow. The inefficiency of charge supply can lead to the formation of "gaps" in the magnetosphere in which the parallel component of electric field is not zero and conditions for particle acceleration exist.

In the case of pulsars, there are several potential ways to supply charged particles to the magnetosphere. First of all, the charge can be extracted directly from the surface of the neutron star. Electrons and positrons can be generated also due to pair production in very strong magnetic field. Finally, electron-positron pairs can be created at interactions of γ -rays with low energy photons.

Apart from the extraction of free charges from the surface of the compact object, the same mechanisms can in principle, be responsible for the charge supply to the magnetosphere in the case of BH. In particular, the pair production of γ -rays in the magnetic field is assumed e.g. in the Blandford-Znajek [13] scenario. The efficiency of this mechanism of charge supply strongly depends on the strength and inclination of the magnetic field (see section 5.3 below). The efficiency of the charge supply via the pair production by γ -rays on the soft infrared background depends on the compactness of the infrared source ($\propto L_{\text{IR}}/R$) [7].

Although in the case of the BHs free charges can not be extracted from the surface of the compact object, the charges can be supplied by the accretion flow. It is not difficult to see that, in general, the charge supply from the accretion flow can also result in the formation of “gaps” in the magnetosphere. A simple illustrative example is given by Fig. 1. Suppose, for example, that the accretion proceeds via a thin equatorial disk (which is a force-free surface for protons in this figure). One can see that extraction of the free charges from the equatorial disk by the rotation-induced electric field will result in the formation of a region filled with electrons, above and below the equatorial disk, up to the conical force-free surface, shown by the black solid thick curve in this figure. However, if the magnetic field is aligned with the rotation axis, the region above the “polar cap” of the BH will remain free of charge, because there is no way to fill this region via extraction of charges from the equatorial disk. Only if the magnetic field is mis-aligned with the BH rotation axis, the free charges from the equatorial disk can “leak” into the polar cap passing through the “reconnection” region of the two force-free surfaces, as it is shown in Fig. 2. This will result in charge supply into the region above the “polar cap”, which is shown as a blue-shaded region in Fig. 1. However, any charged particle which penetrates into this region, escapes to infinity along the magnetic field lines, so that the charge distribution in this region should be constantly “refilled” via the “leakage” from the equatorial force-free surface.

2.3 Geometry and location of the vacuum gap(s).

In the electromagnetic field configuration around the BH discussed in the previous section the vacuum gap forms in the region above the BH “polar cap”,

if the free charges which can fill the magnetosphere are supplied by the equatorial accretion disk. In principle, the re-distribution of the charges supplied from the accretion disk will modify the structure of the electromagnetic field around the BH. The exact location of the vacuum gap(s) in the BH magnetosphere can be found only via numerical modeling of the charge supply and formation of the force-free magnetosphere. Such modeling is difficult already in the case of pulsars, where several “candidate” sites for the vacuum gap locations are considered, such as the magnetic polar cap regions, “slot gaps” at the boundaries of regions filled with positively and negatively charged plasma, “outer gaps” close to the light cylinder etc (see e.g. [8]). In the case of the black holes, modeling of the formation of the force-free magnetosphere has an additional difficulty, because the location of the gap can depend on the geometrical pattern of the accretion flow. The gap model considered in the previous section can serve as a useful “toy model” for the gap geometry.

Within this “toy model” the gap has a particular geometry shown in Fig. 1. Charged particles “leak” from the accretion disk through the region of “reconnection” of the force-free surfaces (see Fig. 2). The gap is situated above the BH “polar cap” and extend along the magnetic field lines up to the height H above the BH horizon. We consider particle acceleration in a gap of such geometry, to establish qualitative features of the vacuum gap acceleration mechanism. Our results can be then generalized, in a straightforward way, to the more complicated (and more realistic) models of vacuum gaps in the black hole magnetosphere.

3 Particle acceleration in the vacuum gap

3.1 General properties of particle motion in the vacuum gap

The electromagnetic field in the vacuum gap consists of electric and magnetic field which are, in general, inclined at a non-zero angle with respect to each other. General properties of particle motion in such electromagnetic field and in the curved space-time around the BH can be readily understood.

Qualitatively, a particle moving in a magnetic field spirals around the magnetic field lines with a giro-radius

$$R_{giro} = \frac{E}{qB_0} \approx 10^2 \left[\frac{10^4 \text{ G}}{B_0} \right] \left[\frac{E}{1 \text{ GeV}} \right] \text{ cm} \quad (12)$$

where E is the energy of the particle and q is its charge. For a particle with an energy $E \ll 10^{20}$ eV the giro-radius is normally essentially less

than the scale of variation of the electromagnetic field which is of order of $R_{\text{Schw}} = 3 \times 10^{13} [M/10^8 M_\odot]$ cm. This giro-radius distance scale is also much smaller than the scale at which particle trajectory is significantly affected by the gravitational field of the black hole (which is also about R_{Schw}). Therefore, one could separate the distance scales at which electromagnetic and gravitational forces are important. At small scales ($\ll R_{\text{Schw}}$) one can locally approximate particle trajectories as motion in the crossed magnetic and electric fields, forming the field configuration described in the Section 2.1.

The motion of a charged particle in such electromagnetic field is composed of the spiraling along the magnetic field lines and the orthogonal drift with velocity

$$v_{\text{drift}} = \frac{\vec{E} \times \vec{B}}{|\vec{B}|^2} \quad (13)$$

Since in the case of interest $|E| \sim |B|$, $v_{\text{drift}} \sim c$ and, in general, particle trajectories significantly deviate from a simple spiraling along the magnetic field lines. For example, the drift velocity of particles moving in the equatorial plane near the black hole placed in the magnetic field, aligned with the black hole rotation axis, is directed along a circle around the black hole, so that the particles drift along the circular trajectories (red circle in the left bottom panel of the Fig. 2). If the magnetic field is slightly mis-aligned with the rotation axis, the particles spiral into (or away from) the black hole, rather than move along the circular orbits (red curves in the middle and right bottom panels of the Fig. 2). The particles, which spiral in, reach the region of “reconnection” of the force-free surfaces (red dots in Fig. 2) and are finally either ejected into the “polar cap” region or fall under the BH horizon.

Apart from spiraling along the magnetic field lines and drift across the field lines, particles can be accelerated by the electric field. Only the presence of electric field component along the magnetic field line can lead to the increase or decrease of particle energy. Obviously, positively charged particles are accelerated in the direction opposite to the direction of acceleration of negatively charged particles. Depending on the location of the point of injection of a low-energy particle (e.g. proton or electron) into the reconnection region, the particle can be accelerated in such a way that it either escapes “to infinity” along the direction of magnetic field lines, or it is trapped in a finite region between the neighbouring force-free surfaces close to the horizon.

3.2 Maximal energies of accelerated particles

Neglecting the energy losses, the maximal energies attainable for nuclei of the charge Ze are determined by the available potential difference in the gap, $U \sim ER \sim aBR$,

$$E_{\max} = ZeBR \simeq 10^{20} Z \left[\frac{B}{10^4 \text{ G}} \right] \left[\frac{M}{10^8 M_{\odot}} \right] \text{ eV}. \quad (14)$$

In a realistic situation the energy losses of the accelerated particles (e.g. on the electromagnetic radiation associated with the accelerated motion of the particle) limit the maximal energies to the values below the estimate of Eq. (14).

In particular, the accelerated nuclei inevitably suffer from the curvature radiation loss

$$\frac{dE}{dt} = -\frac{2Z^2 e^2 E^4}{3A^4 m_p^4 R^2}, \quad (15)$$

where m_p is the proton mass and A is the atomic number. In the electromagnetic field configuration (5), describing a magnetic field almost aligned with the BH rotation axis, the curvature radius of magnetic field lines in the gap scales roughly as $R \simeq R_{\text{Schw}}/\chi$. This translates into the following maximum energy,

$$E_{\text{cur}} = \left[\frac{3A^4 m_p^4 R^2 B}{2Ze\chi^2} \right]^{1/4} \simeq 8 \times 10^{19} A Z^{-1/4} \left[\frac{M}{10^8 M_{\odot}} \right]^{1/2} \left[\frac{B}{10^4 \text{ G}} \right]^{1/4} \left[\frac{\chi}{1^\circ} \right]^{-1/2} \text{ eV}. \quad (16)$$

The range of applicability of Eq. (16) is given by the condition $B > B_{\text{crit}}$, where B_{crit} is found from the requirement $E_{\text{cur}} = E_{\max}$:

$$B_{\text{crit}} = \left[\frac{3A^4 m_p^4}{2Z^5 e^5 R^2 \chi^2} \right]^{1/3} \simeq 10^4 A^{4/3} Z^{-5/3} \left[\frac{M}{10^8 M_{\odot}} \right]^{-2/3} \left[\frac{\chi}{1^\circ} \right]^{-2/3} \text{ G}. \quad (17)$$

This critical field corresponds to particle energy

$$E_{\text{crit}} \approx 10^{20} A^{4/3} Z^{-2/3} \left[\frac{M}{10^8 M_{\odot}} \right]^{1/3} \left[\frac{\chi}{1^\circ} \right]^{-2/3} \text{ eV}, \quad (18)$$

The above estimates show that it is possible to accelerate protons or heavier nuclei to the energies about 10^{20} eV in the central engines of typical AGNs, with the BH masses around 10^8 solar masses. The necessary condition for such acceleration is that the curvature radius of particle trajectories should be much larger (by a factor $1/\chi$) than R_{Schw} . This can be achieved in the “polar cap” regions, if the magnetic field is moderately misaligned with the BH rotation axis.

4 Numerical modeling of particle acceleration in the gap

In order to study the dependence of the maximal energies of the accelerated particles on the parameters of the model (in particular, on the BH mass M , magnetic field B and inclination angle χ of the magnetic field with respect to the BH rotation axis), we have developed a numerical code which traces the particle trajectories through the electromagnetic field configuration described in Section 2 with the account of the energy loss on the emission of synchrotron/curvature radiation. To study the electromagnetic luminosity of the vacuum gap we also model the propagation of photons emitted by the accelerated particles through the BH space-time.

4.1 Numerical code

We have developed a numerical code to model charged particle motion in the curved space-time and in the electromagnetic field configuration described Section 2.1. For this we have first written the equations of motion of a charged particle in the LNRF (see Eq. 7) [18]

$$\frac{d\vec{p}}{dt} = e(\vec{E} + \vec{v} \times \vec{B}) + m\gamma\vec{g} + \hat{H}\vec{p} + \vec{f}_{rad} \quad (19)$$

where \vec{p} is the particle momentum

$$p^{\hat{a}} = m\gamma v^{\hat{a}} \quad (20)$$

(hats denote the vector components in the LNRF) \vec{g} is the gravitational acceleration and \hat{H} is the tensor of gravi-magnetic force. The force \vec{f}_{rad} is the radiation reaction force and $v^{\hat{a}}$ is the 3-velocity of the particle in the LNRF. Next, taking into account the fact that the motion of a charged particle involves many distance scales, from the giroradius R_{giro} (12) up to R_{Schw} , we have found that a step of the numerical integration is determined by the smallest scale involved (R_{giro} most of the time). At this length scale the motion of

the particle can be modelled in the LNRF by a numerical integration of Eqs. (20). Using the book [31], we have written a code, which integrates the above equations numerically. The elementary step of the numerical integration increases or decreases along the particle trajectory, together with the increase or decrease of the energy of the particle (see Eq. 12).

The radiation reaction force \vec{f}_{rad} for the ultra-relativistic particles moving in external electromagnetic field is (see, e.g. [32])

$$\vec{f}_{rad} = \frac{2e^4\gamma^2}{3m^2} \left((\vec{E} + \vec{v} \times \vec{B})^2 - (\vec{v} \cdot (\vec{E} + \vec{v} \times \vec{B}))^2 \right) \frac{\vec{v}}{|\vec{v}|} \quad (21)$$

Note that if particles move at large angle with respect to the magnetic field lines, this expression will describe mostly synchrotron energy loss. However, in the case when particles move almost along the magnetic field lines, the last equation will "mimic" the effect of curvature energy loss.

We follow the particle trajectories during the phase of in-spiralling along the equatorial plane and subsequent propagation inside the vacuum gap. The particles are supposed to be initially at rest, with respect to the LNRF. Particles are initially injected in the equatorial plane (to mimic the injection from the thin accretion disk).

To study the electromagnetic emission from the accelerated particles we calculate, at each step of the integration of particle trajectory, the energy and power of synchrotron/curvature emission and ascribe this energy and power to a nominal "photon" which is emitted along the direction of the particle motion. We subsequently trace the trajectory of each emitted photon from the emission point to infinity by integrating the equations of the geodesics of the Kerr metric.

Charged particles which reach the outer boundary of the gap, escape along the geodesics of the Kerr metric. The motion along the time-like geodesics of the Kerr metric is determined by the equations [33]

$$\begin{aligned} r^2 \dot{r} &= \sqrt{T^2 - \Delta(\mu^2 r^2 + (\Phi - aE)^2)} \\ r^2 \dot{\phi} &= \Phi - aE + aT/\Delta \\ r^2 \dot{t} &= a\Phi - a^2 E + (r^2 + a^2)T/\Delta \end{aligned} \quad (22)$$

where E and Φ are the integrals of motion, which correspond to the conserved energy and angular momentum, μ is particle mass and T is defined as $T = E(r^2 + a^2) - \Phi a$. In the following, the cited energies of particles ejected from the gap are always the "energies measured by an observer at infinity", i.e. the integrals of motion E , which enter the geodesic equations (22).

4.2 Dependence of the maximal energy on the gap parameters

In this section we study dependence of maximum energy to which protons can be accelerated on the geometry of the gap, namely, on the basic parameters of the model: the gap height H , the inclination of magnetic field with respect to the BH rotation axis, χ , the BH mass M and on magnetic field strength B .

Fig. 3 shows the dependence of maximum energy of accelerated protons on the gap height H . We set the inclination angle of magnetic field $\chi = 3^\circ$. One can see that for the assumed BH mass, $M_{\text{BH}} = 3 \times 10^8 M_\odot$, the acceleration to the energies above 10^{20} eV is possible only if the gap height is larger than $H > R_{\text{Schw}}$, provided that the magnetic field near the horizon is extremely strong, $B > 3 \times 10^4$ G. One can notice that the increase of the gap height beyond a certain field-dependent limit does not lead to the further increase of the particle energies. This is explained by the decrease of the electric field strength (see Eq. 10) and, as a consequence, the decrease of the acceleration rate far from the BH. Since the magnetic field is assumed to be asymptotically constant, the rate of the energy loss does not decrease with the distance, contrary to the acceleration rate. The combination of the decreasing acceleration rate and steady loss rate leads to the decrease of the particle energies at large distances. Obviously, the assumption of the asymptotically constant magnetic field, adopted in our toy model, does not hold in a realistic case, when the magnetic field is produced by the accreting matter.

Fig. 4.2 shows the dependence of maximum energy on the inclination angle of magnetic field with respect to the rotation axis of the black hole, χ . In our toy model, particles are initially supplied by the equatorial accretion disk, so that the initial positions of the particles are in the equatorial plane. One can see that the acceleration to the energies above 10^{20} eV close to a BH of the mass $5 \times 10^8 M_\odot$ is possible only if $\chi \ll 1$. The increase of the misalignment between the magnetic field and the BH rotation axis leads to the decrease of the maximal energies and to the increase of the power of electromagnetic emission which accompanies the acceleration process ((cyan dashed curves in this Figure are marked by the value of the ratio of the electromagnetic luminosity, L_{EM} to the UHECR luminosity, L_{UHECR}).

The requirement on the alignment of the magnetic field can be somewhat relaxed in the case of higher black hole mass or still higher magnetic field strength. In fact, since, in the "energy loss saturated" regime the maximal energy grows as $B^{1/4} M^{1/2}$ (see Eq. 16), the increase of the magnetic field by an order of magnitude results just in a slight correction of the maximal allowed misalignment angle, while an order of magnitude heavier black hole accelerates particles to just a factor of 3 higher energies.

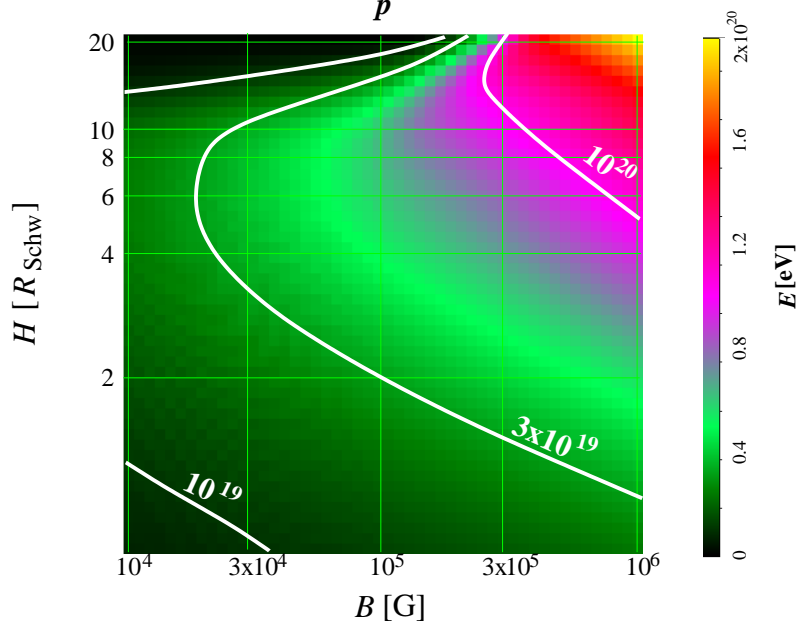


Fig. 3. Energies of protons ejected from the vacuum gap (measured by an observer at infinity), as a function of the gap height H and magnetic field B . The parameters are: BH mass $M = 3 \times 10^8 M_\odot$, rotation moment per unit mass $a = 0.99GM$, the inclination angle of magnetic field $\chi = 5^\circ$. Protons are initially injected in the equatorial plane at the distance $R = 1.4r_H$ from the BH.

This is clear from Fig. 5 in which the dependence of the particle energies on the magnetic field and the BH mass is shown. From this Figure one can see that at the energies $E \geq 10^{20}$ eV the relation (16) holds, so that at the levels $E = \text{const}$ one has $M \sim B^{-1/2}$. For a $10^9 M_\odot$ BH the energy 10^{20} eV is attainable already when the magnetic field is $B \sim 10^4$ G. However, the further increase of the magnetic field by two orders of magnitude, up to $B \sim 10^6$ G, results in an increase of the particle energies just by a factor of 2.

5 Electromagnetic emission from the gap

5.1 Direct γ -ray emission from the particle acceleration in the gap

Protons accelerated near the BH horizon in the gap can produce γ -ray emission in the VHE band through several radiation mechanisms. For example, TeV emission can be synchrotron or curvature γ -ray emission which accompanies proton acceleration [4,6]. The energy of curvature photons produced by

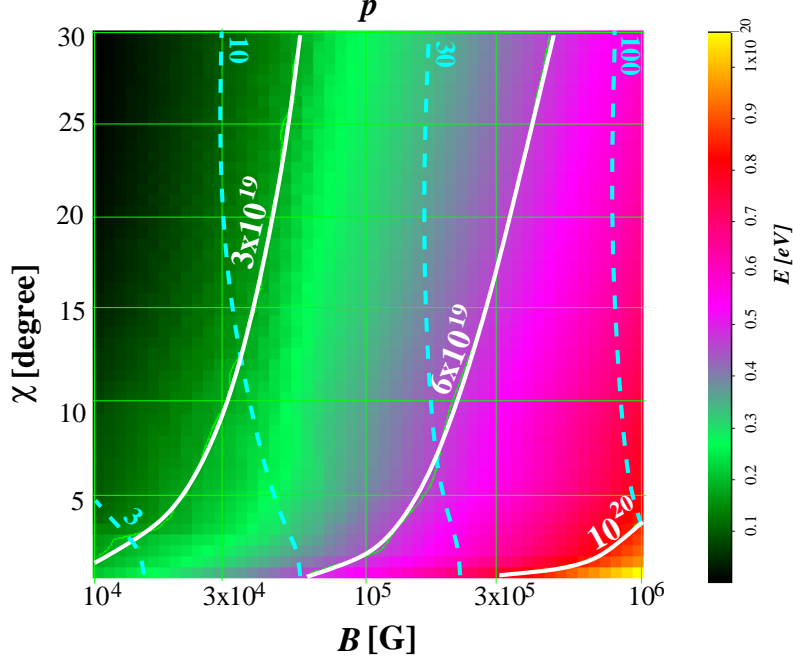


Fig. 4. Energies of protons ejected from the vacuum gap (measured by an observer at infinity), as a function of the inclination angle of magnetic field, χ and of the magnetic field strength B . The parameters of the calculation are: $M = 3 \times 10^8 M_\odot$, $a = 0.99GM$, $H = 5R_{\text{Schw}}$. Dashed cyan contours show the ratio of the electromagnetic to cosmic ray luminosity for the particular gap parameters.

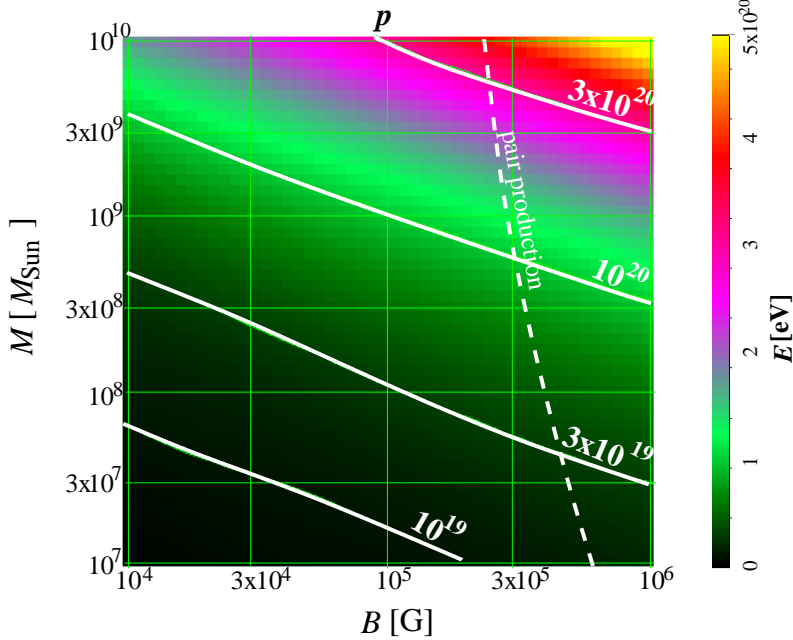


Fig. 5. Maximal energy of protons ejected from the vacuum gap (measured by an observer at infinity), as a function of the BH mass M and magnetic field B . The parameters are: $a = 0.99GM$, $\chi = 5^\circ$, $H = 5R_{\text{Schw}}$. Particles are initially injected in the equatorial plane at the distance $R = 1.4r_H$ from the BH.

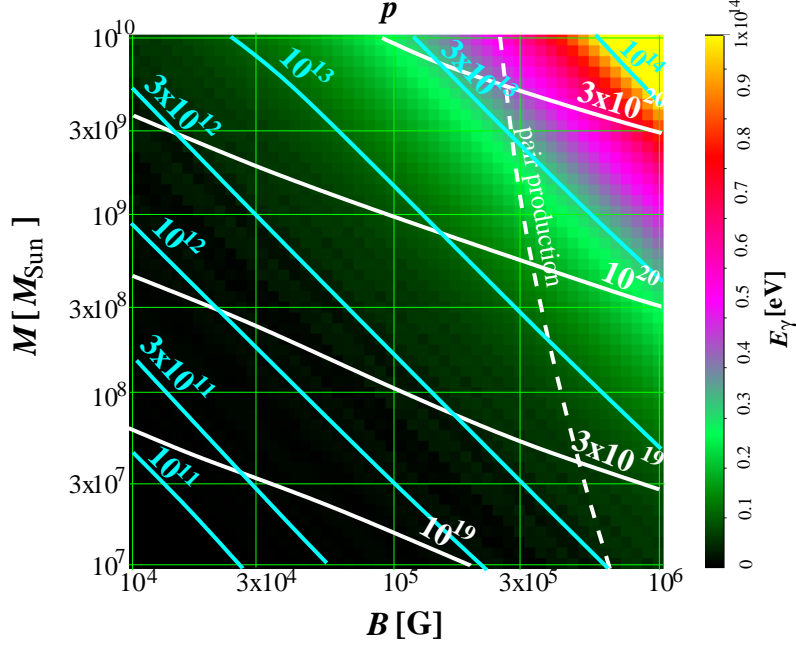


Fig. 6. Color and cyan contours: maximal energy of gamma quanta produced by the accelerated protons in the vacuum gap (measured in the LNRF), as a function of the BH mass and magnetic field. White contours show the maximal energies of the accelerated protons (see Fig. 5). Dashed line shows the values of M, B at which the pair production in the magnetic field sets on on the distance scale of the inhomogeneity of the magnetic field. The parameters are: $a = 0.99GM$, $\chi = 5^\circ$, $H = 5R_{\text{Schw}}$. Protons are initially injected in the equatorial plane at the distance $R = 1.4r_H$ from the BH.

protons accelerated to the energy E_{curv} , given by Eq. (16), is and

$$\epsilon_{\text{curv},p} \simeq 2 \left[\frac{E_{\text{curv}}}{10^{20} \text{ eV}} \right]^3 \left[\frac{M}{3 \times 10^8 M_\odot} \right]^{-1} \left[\frac{\chi}{1^\circ} \right] \text{ TeV} \quad (23)$$

Thus, particle acceleration activity of the gap should reveal itself through the γ -ray emission in the very-high-energy (VHE) band. Fig. 6 shows numerically calculated dependence of the maximal energies of the γ -rays emitted by the gap on the physical parameters of the gap, M, B . One can see that for the range of parameters at which UHECR production is possible (i.e. above the thick white line with the mark "10²⁰" in this figure) the maximal energies of the γ -rays reach 1 – 100 TeV. Combining Eqs. 16 and 23 one can find that $\epsilon_{\text{curv},p} \sim M^{1/2} B^{3/4}$ so that the lines $\epsilon_{\text{curv},p} = \text{const}$ correspond to $M \sim B^{-3/2}$ in the figure.

The "direct" γ -ray emission from the vacuum gap is highly anisotropic (in fact the opening angle of the emission cone is determined not only by the width of the gap, but also by the deflections of the γ -ray trajectories by the BH gravitational field. Fig. 7 shows the angular distribution of the average

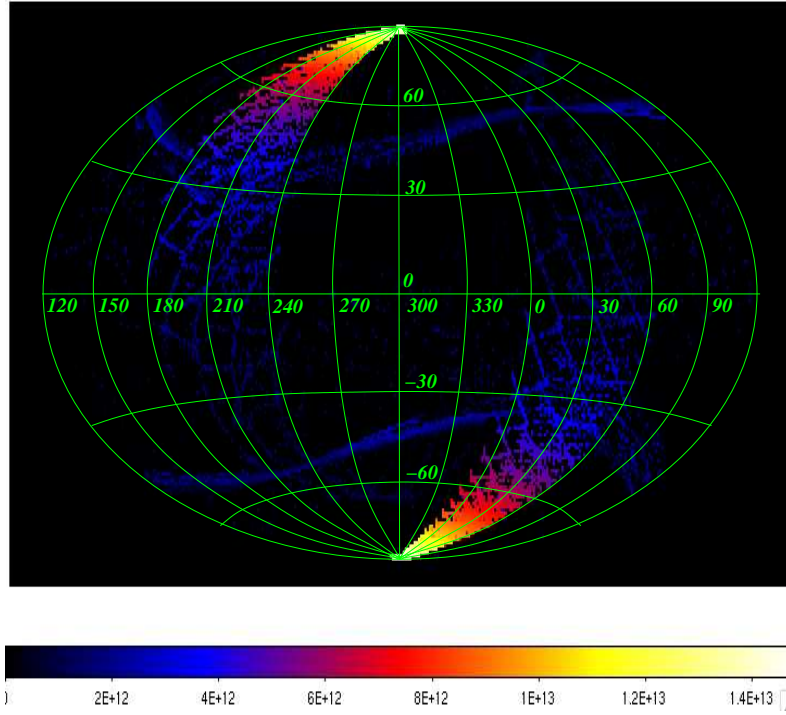


Fig. 7. Anisotropy pattern of the γ -ray emission from the gap. The parameters are: $a = 0.99GM$, $\chi = 5^\circ$, $H = 5R_{\text{Schw}}$. Particles are initially injected in the equatorial plane at the distance $R = 1.4r_H$ from the BH.

energies of the γ -rays emitted by particles accelerated in the gap. The highest energy photons are emitted in the direction of the magnetic field. The inspiralling particles penetrate into the reconnection region mostly from the two opposite directions in the equatorial plane, in which the reconnection of the force-free surfaces starts at the largest distance (see the bottom panels of Fig. 2). This explains the appearance of the two emission regions at the opposite sides of the black hole. The highest energy γ -rays are emitted in the directions of the southern and northern poles, along the direction of the magnetic field. Lower energy photons emitted closer to the equatorial plane are more strongly deviated and absorbed by the BH. A characteristic anisotropy of the γ -ray emission from the gap is preserved even if the magnetic field is not aligned with the BH rotation axis (see e.g. [7]).

In most of the sources the magnetic field in the gap is not aligned with the line of sight toward the source, so that the direct γ -ray emission from the gap is not detectable. However, the 0.1-100 TeV γ -ray flux from the gap can be efficiently "recycled" and "isotropized" via the development of electromagnetic cascade in the infrared-to-ultraviolet photon background in the source (see e.g. [7]). This should lead to the redistribution of the primary γ -ray power over the lower energy photons, from radio to softer γ -rays. The details of the resulting cascade spectrum depend on the details of the soft photon and

particle distributions in the particular sources.

5.2 Power of direct γ -ray emission from the gap

The UHECR data [21] imply that the total flux of the cosmic rays above the cut-off at $E \sim 10^{20}$ eV is about ¹

$$F(E > 10^{20} \text{ eV}) \simeq (0.3 \div 1) \times 10^{-12} \text{ erg/cm}^2\text{s} \quad (24)$$

If this flux is produced by $N_{\text{source}} \sim 100$ UHECR sources at the distances $D \sim 50 \div 100$ kpc, the typical luminosity of an UHECR source is about

$$L_{\text{source}} \simeq (10^{40} \div 10^{41}) \left[\frac{100}{N_{\text{source}}} \right] \text{ erg/s} \quad (25)$$

Such an estimate should be compared to an estimate of the power of the UHECR emission by a typical vacuum gap close to a supermassive BH in AGN, which can be obtained in the following way. At small inclination angles χ the area of the region of the reconnection of the force-free surfaces in the equatorial plane (see Fig. 2) is estimated as $A \sim 2\pi r_H^2 \sin \chi$. The maximal rate of injection of the charged particles into the gap through the reconnection region is

$$R_{\text{max}} \simeq n_{GJ} A \quad (26)$$

where n_{GJ} is filled with the Goldreich-Julian density, given by the Eq. 11. The energy of each particle ejected from the gap is E_{curv} , given by the Eq. 16. This means that the maximal cosmic ray power of the gap is

$$L_{\text{CR,max}} \simeq R_{\text{max}} E_{\text{curv}} \simeq 6 \times 10^{42} A Z^{-5/4} \left[\frac{M}{10^8 M_{\odot}} \right]^{3/2} \left[\frac{B}{10^4 \text{ G}} \right]^{5/4} \left[\frac{\chi}{1^\circ} \right]^{1/2} \text{ erg/s} \quad (27)$$

where we have assumed $\theta \simeq \chi$. Comparing the estimate (25) to (27) one can see that the necessary cosmic ray power of the vacuum gaps near the supermassive BHs can be achieved already when the charged particles are injected into the gap at the rate $\sim (0.01 - 0.1) R_{\text{max}}$.

If the sources of UHECR are supermassive BHs in the centers of galaxies, the acceleration to the energies above 10^{20} eV is possible only in the “loss

¹ This estimate is almost an order of magnitude lower than the one used in the Ref. [6] which relied on the AGASA data which did not show a signature of cut-off.

saturated” regime, in which the acceleration rate is balanced by the energy loss rate, for most of the trajectory of the particle. This means that the power of electromagnetic emission from the gap dominates over the power emitted in the form of the high-energy particles.

Even in the case of the almost aligned magnetic field, considered in this paper, the power of electromagnetic emission from a (*several*) $\times 10^8 M_\odot$ BH is at least by a factor of $10 \div 50$ larger than the UHECR power, as soon as the energy 10^{20} eV is reached (see Fig. 8). From this figure one can see that the lines $L_{\text{EM}}/L_{\text{UHECR}} = \text{const}$ roughly correspond to $M \sim B^{-3/2}$. This behaviour is readily explained, if one takes into account that a simple estimate of $L_{\text{EM}}/L_{\text{UHECR}}$ can be obtained by comparing the total available potential difference in the gap to its fraction, spent on the particle acceleration (rather than on the electromagnetic emission)

$$\frac{L_{\text{EM}}}{L_{\text{UHECR}}} \simeq \frac{E_{\text{max}}}{E_{\text{cur}}} \simeq 1 Z^{5/4} A^{-1} \left[\frac{M}{10^8 M_\odot} \right]^{1/2} \left[\frac{B}{10^4 \text{ G}} \right]^{3/4} \left[\frac{\chi}{1^\circ} \right]^{1/2} \quad (28)$$

If the magnetic field is aligned with the rotation axis, $\chi \ll 1$, the estimate of the electromagnetic power is much lower than the one found for a general case of misaligned magnetic field in the Ref. [6]. This means that a typical electromagnetic luminosity of a nearby UHECR source is

$$L_{\text{EM, source}} \geq (10 \div 100) L_{\text{source}} \sim (10^{41} \div 10^{43}) \left[\frac{100}{N_{\text{source}}} \right] \text{ erg/s} \quad (29)$$

Such a luminosity is at the level of the luminosities of the AGN in the local Universe.

The primary power emitted in the form of the VHE γ -rays is, most probably, recycled via the cascading on the infrared backgrounds in the AGN central engine and in the host galaxy of the source. The cascading leads to the isotropization of the secondary emission, so that an observer is still able to detect a certain fraction of the primary power in the form of lower energy (e.g. synchrotron or inverse Compton) photons from the electromagnetic cascade.

5.3 Maximal height of the vacuum gap

The VHE γ -rays emitted by the accelerated particles can be absorbed in interactions with soft background photons or with magnetic fields. e^+e^- pairs produced in these interactions could initiate a development of electromagnetic cascade in the gap which finally can “short circuit” the vacuum gap and neutralize the parallel component of the electric field via charge redistribution.

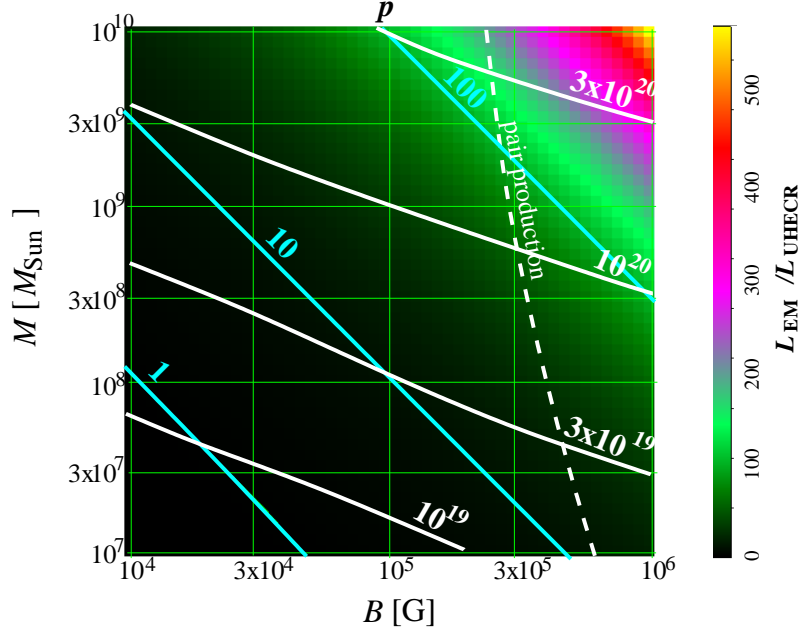


Fig. 8. Ratio of the electromagnetic to the cosmic ray power of the gap, as a function of the BH mass M and magnetic field B . White contours show the maximal energies of the accelerated protons (see Fig. 5). The parameters are: $a = 0.99GM$, $\chi = 5^\circ$, $H = 5R_{\text{Schw}}$. Particles are initially injected in the equatorial plane at the distance $R = 1.4r_H$ from the BH.

Similarly to the case of vacuum gaps in the pulsar magnetospheres, the condition that the high-energy gamma-ray quanta emitted from the gap do not produce e^+e^- pairs either in interaction with the strong magnetic field or with the soft background photons can limit the height of the gap. Requiring that the gap height H is smaller than the mean free path of a γ ray through the magnetic field, one finds [34]

$$H \leq D_{B\gamma} \approx 95 \left[\frac{10^4 \text{ G}}{B_\perp} \right] \exp(8m_e^3/3B_\perp \epsilon_{\text{curv}}) \text{ cm} \quad (30)$$

In the case when the magnetic field is almost aligned with the black hole rotation axis, the γ -rays are emitted along the direction of propagation of the accelerated particles, which, in turn, move along the magnetic field lines. This means that the typical normal component of the magnetic field is

$$B_\perp \sim B \sin \chi \quad (31)$$

so that for the case $\chi \sim 1^\circ$, considered here, the magnetic field component orthogonal to the particle and γ -ray velocity is some 2 orders of magnitude weaker than the parallel one. This means that even if the magnetic field in the vacuum gap is very strong, $B \sim 10^6$ G, the typical mean free path of the γ -rays is larger than the characteristic distance scale of the problem (the

Schwarzschild radius, R_{Schw}). Thus, in the considered case of the gap with “aligned” magnetic field, the pair production is not important over the entire range of BH masses studied in this paper. To check this conclusion we have included in the numerical code a calculation of the mean free path of the γ -rays emitted at each step of the particle trajectory and checked that the condition (30) is never violated when the acceleration to the energies above 10^{20} eV is possible in the range of parameters M, B, H and χ considered above.

Instead, in a realistic situation, the height of a vacuum gap with aligned magnetic field is most probably limited by the large-scale variations of the magnetic field, created by the accretion flow. Assuming that the magnetic field has a certain inhomogeneity scale R_B , one can find that the change of the field direction on this distance scale will lead to the loss of alignment between the trajectories of the γ -rays emitted by particles accelerated in the gap and the magnetic field, so that the normal component of the magnetic field becomes $B_{\perp} \sim B$. We have calculated the magnetic field strength at which the pair production on the distance scale R_B can set on, by substituting B instead of B_{\perp} in the estimate of Eq. 30 in numerical calculations. As a result, we have found that the pair production can set on if the magnetic field strength is above the threshold shown by a white dashed line in Fig. 8. One can see that in the case when the magnetic field in the gap is aligned with the BH rotation axis, the pair production on the distance scale of inhomogeneity of the magnetic field can set on at the magnetic field strengths, $B \geq 10^5$ G.

6 Acceleration of heavy nuclei

Up to now we have considered the acceleration of protons. However, our results can be generalized, in a straightforward way, to the case of acceleration of heavier nuclei, using the equations of Section 3.2.

Heavy nuclei, like the fully ionized iron, could be accelerated to higher energies, since their charge is $Z > 1$. However, nuclei with energies above 10^{20} eV are easily disintegrated in interactions with the infrared background photons which are present at the acceleration site, in the accelerator host galaxy, in the intergalactic space and in the Galaxy. The secondary nucleons produced in the photon disintegration, have the energy $E_N \simeq E/A$. Taking this into account, one can find that, if the nuclei are fully disintegrated, the assumption about the acceleration of nuclei does not result in the increase of the estimate of the maximal energies of protons reaching the detector on the Earth. E.g. the critical energy (per nucleon), at which the transition to the loss-dominated regime of acceleration happens (see Eq. 18),

$$E_{\text{crit},N} \simeq E_{\text{crit}}/A \sim A^{1/3} Z^{-2/3} \quad (32)$$

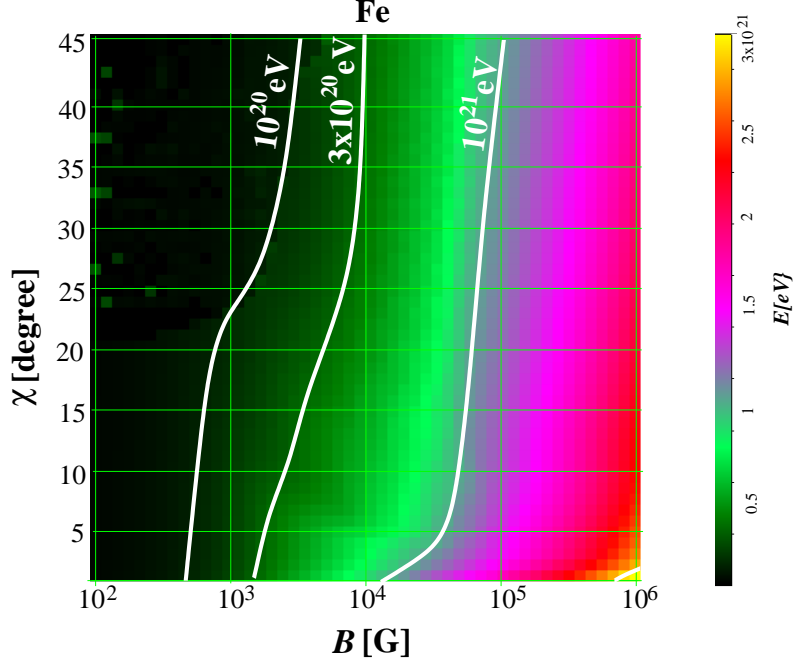


Fig. 9. Same as in Fig. 4.2 but for the case of acceleration of the iron nuclei.

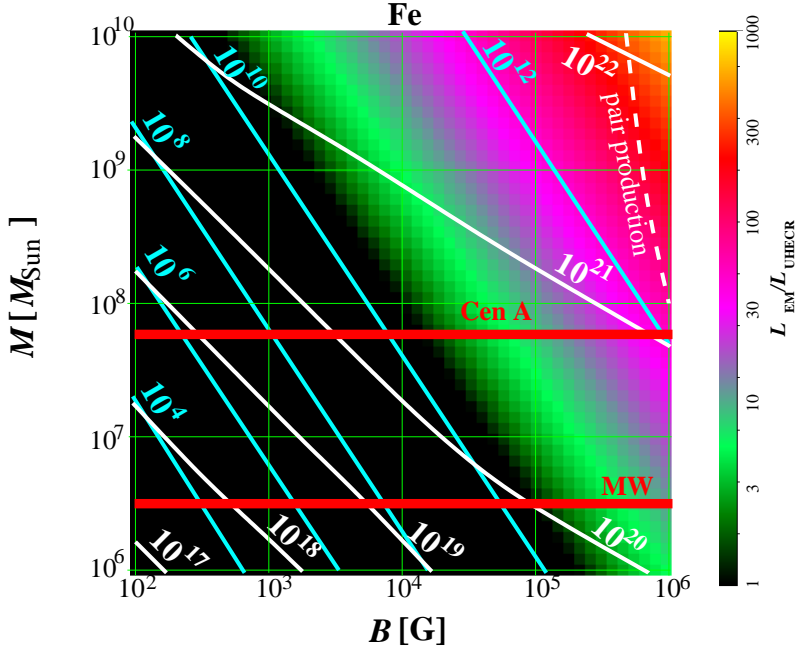


Fig. 10. Same as in Fig. 8 but for the case of acceleration of iron nuclei. The masses of the BH in the center of the Milky Way and in the nucleus of Cen A are marked by red horizontal lines. The white contours show the maximal energies of the accelerated Fe nuclei (in eV). Cyan contours show the maximal energies of the γ -rays emitted by the nuclei (in eV). White dashed line shows the limit at which the pair production on the distance scale of inhomogeneity of the magnetic field sets on.

scales as $A^{1/3}Z^{-2/3}$, the factor which is less than 1 for most of the primary nuclei. In the case of acceleration in the curvature loss dominated regime, $E_{\text{cur,N}} \simeq E_{\text{cur}}/A \sim Z^{-1/4}$ does not depend on the atomic number A at all.

However, the assumption about full disintegration of the nuclei on the way from the source to the observer on the Earth can be not valid in some particular cases. First, if the energies of the Fe nuclei are around 10^{20} eV, the mean free path of the nuclei through the extragalactic infrared photon background is ~ 100 Mpc. This means that the nuclei accelerated near the supermassive BH in the nearby galaxies can cover the entire distance from the host galaxy to the Milky Way without being photo-disintegrated [35]². Next, if the heavy nuclei are accelerated close to the supermassive BH in the center of the Milky Way galaxy, they also can reach the Earth without being photo-disintegrated.

The case of the acceleration of the heavy nuclei differs from the case of proton acceleration in two important aspects: the higher mass of the nucleus (and, respectively, lower Lorentz factor) result in the reduction of the rate of the curvature energy loss and of the energies of the quanta of curvature radiation. Because of the lower energies of the curvature radiation quanta, the pair production, which could limit the size of the gap (see previous Section), sets on at higher values of the magnetic field. In addition, the electromagnetic luminosity of a source accelerating nuclei to the energies $\sim 10^{20}$ eV could be lower, than that of the source accelerating protons to $\sim 10^{20}$ eV.

Figs. 9 and 10 show the numerically calculated maximal energies of accelerated particles and ratio of the electromagnetic to UHECR luminosity, as a function of M, B, χ , in the case of acceleration of Fe nuclei. The region of parameter space in which the acceleration proceeds in the “loss free” regime (i.e. the estimate of the maximal energy is given by Eq. 14) is the black triangle in the lower left corner of the figure. One can see that in spite of the moderate BH masses (down to $M \sim 10^7 M_\odot$) and/or moderate magnetic fields (down to $B \sim 10^3$ G in the case of a $10^9 M_\odot$ BH), the acceleration up to the energies $> 10^{20}$ eV is possible in this regime.

As an example, let us consider the particularly interesting case of particle acceleration near the supermassive BH in the center of the Milky Way galaxy, which hosts a BH of the mass $M \sim 3 \times 10^6 M_\odot$ [36] (horizontal red line in Fig. 10). From Fig. 10 one can see that such a BH can accelerate iron nuclei up to the energies $\sim 10^{19}$ eV if the magnetic field around it reaches $B \sim 5 \times 10^3$

² One should note that in a model in which the UHECR events are assumed to be Fe nuclei, correlation of the arrival directions of the highest energy events with their AGN sources, like the one reported in the Ref. [25], is not expected, unless the ordered Galactic magnetic field is unnaturally weak. Besides, one has to assure that UHECR nuclei are not destroyed by the infrared background in the source host galaxies.

G. The energy loss in this case is much smaller than the power of the cosmic ray emission $L_{\text{EM}}/L_{\text{UHECR}} = 5 \times 10^{-4}$. Fe nuclei with the energies 10^{18-19} eV produced in the Galaxy are assumed to dominate the cosmic ray flux in this energy band in certain models explaining the “ankle” feature of the cosmic ray spectrum [37]. In order to explain the observed cosmic ray flux at 10^{18} eV $F(10^{18} \text{ eV}) \simeq 200 \text{ eV}/(\text{cm}^2 \text{ s sr})$ [21], the cosmic ray luminosity of a source in the Galactic Center should be $L_{\text{Fe}} \sim 3 \times 10^{36} \text{ erg/s}$ (the luminosity can be still lower if the Fe nuclei diffuse through the Galactic magnetic field). From Fig. 10 one can see that the power of electromagnetic emission, which accompanies iron nuclei acceleration, could be as low as $L_{\text{EM}} \leq 10^{-3} L_{\text{Fe}}$, which is much less than the observed luminosity of the Galactic Center in the TeV band ($\sim 10^{35} \text{ erg/s}$ [38]). Of course, relaxing the assumption of approximate alignment of magnetic field with the BH rotation axis would result in a higher estimate of the electromagnetic luminosity. However, as it is clear from Eq. 28, even in the loss-saturated regime of particle propagation in the gap, the power of electromagnetic emission increases by a factor of ~ 10 as the inclination angle of magnetic field increases from several degrees to $\chi \sim 1$. Thus, even in the absence of alignment of the magnetic field, the electromagnetic emission which would accompany acceleration of the iron nuclei to the energies $\sim 10^{18-19}$ eV close to the Galactic Center BH would not be accompanied by significant electromagnetic emission.

7 Discussion and conclusions

In this paper we have considered proton and heavy nuclei acceleration in the vicinity of the horizon of the supermassive BHs. We have shown that proton acceleration by a large scale electric field induced by the rotation of the BH can result in the production of cosmic rays with energies above 10^{20} eV, provided that the magnetic field in the acceleration region is almost aligned with the BH rotation axis (to better than few degrees, for a reasonable range of black hole masses and magnetic field strengths $10^8 M_{\odot} \leq M_{\text{BH}} \leq 10^{10} M_{\odot}$, $10^4 \text{ G} \leq B \leq 10^6 \text{ G}$).

We have found that in a particular case of a rotating BH accreting through an equatorial disk, the vacuum gaps, in which the large-scale electric field is not neutralized by redistribution of charges, form above the polar cap regions of the BH (see Fig. 1). In the case of magnetic field exactly aligned with the BH rotation axis, charged particles from the equatorial accretion flow can not penetrate into the polar cap regions (and, therefore, can not be accelerated). However, as soon as the magnetic field is mis-aligned with the BH rotation axis, the charged particles which are initially injected at large distances into the equatorial plane, drift along the equatorial plane toward the BH, until they reach the region of “reconnection” of the force-free surfaces close to the

BH horizon (Fig. 2). As soon as the particles from the equatorial plane penetrate into the reconnection region, they "leak" into the vacuum gaps above the polar caps and are ejected to infinity with high energies. Numerical modeling of particle transport and acceleration close to the BH has enabled us to calculate the dependence of the maximal attainable energies of the accelerated particles, as well as of the properties of electromagnetic emission produced by the accelerated particles on the physical parameters, such as the BH mass M , the magnetic field B , the inclination of the magnetic field χ and the gap height H (see Figs. 3, 4.2, 5, 6, 8).

We have found that if the magnetic field is aligned to within several degrees with the rotation axis, the electromagnetic luminosity of the gap is just 10-50 times larger as compared its UHECR ($E > 10^{20}$ eV) proton luminosity. A simple estimate has led us to a conclusion that the resulting electromagnetic luminosity of the gap is of the order of the bolometric luminosity of a typical AGN in the local Universe, which makes the central engines of the AGN plausible candidates for the astrophysical UHECR sources.

In the case of acceleration of heavy nuclei, acceleration to the energy $\geq 10^{20}$ eV is possible for a much wider range of BH masses and magnetic fields, without strong requirement on alignment (see Fig. 9). In particular, even a BH of the mass $\sim 3 \times 10^6 M_\odot$ (like the one in the center of the Milky Way galaxy, [39]) can accelerate iron nuclei to the energies above 10^{18} eV when the magnetic field is several hundred Gauss, in the regime when the power of electromagnetic emission from the accelerator is negligible, compared to its cosmic ray power. Similarly, the nearest AGN Centaurus A, which hosts a BH with the mass $\sim 6 \times 10^7 M_\odot$ [40] can produce Fe nuclei with the energies 10^{20} eV if the magnetic field close to the BH horizon is above 3×10^3 G. (see Fig. 10). It is important to understand how often the strong alignment between the magnetic field and BH spin, $\zeta < (several)^\circ$, arises in AGN. This will help to discriminate between proton and heavy nuclei at highest energies, $E \geq 10^{20}$ eV.

The energy spectra of cosmic rays produced by individual sources via the considered particle acceleration mechanism are sharply peaked at nearly maximum energy, similarly to the spectra of high-energy particles produced in linear accelerators. This feature can potentially distinguish the presented mechanism from conventional shock acceleration mechanism, which typically gives power law spectra $dN/dE \sim E^{-\alpha}$ with $\alpha \geq 2$. The typical intrinsic spectra of the UHECR sources can be found with a higher statistics of the UHECR events, $N > 100$ events at $E > 60$ EeV [41].

References

- [1] F. A. Aharonian et al., *Science* **314**, 1424, (2006).
- [2] J. Albert et al., *Ap.J.*, **669**, 862, (2007).
- [3] F. Aharonian et al., *Ap.J.*, **664**, L71, (2007).
- [4] A. Levinson, *Phys. Rev. Lett.*, **85**, 912 (2000).
- [5] F. A. Aharonian, A. A. Belyanin, E. V. Derishev, V. V. Kocharovsky and V. V. Kocharovsky, *Phys. Rev. D*, **66**, 023005 (2002). [arXiv:astro-ph/0202229].
- [6] A. Neronov, P. Tinyakov and I. Tkachev, *J. Exp. Theor. Phys.*, **100**, 656, (2005) [*Zh. Eksp. Teor. Fiz.*, **100**, 744, (2005)].
- [7] A. Neronov and F. Aharonian, *Ap.J.*, **671**, 85 (2007).
- [8] Lyne A. & Graham-Smith F. *Pulsar Astronomy* Cambridge Univ. Press (2005).
- [9] R.M.Wald, *Phys.Rev. D* **10**, 1680, (1974).
- [10] J.Bicak, L.Dvorak, *Gen.Rel.Grav.*, **7**, 959, see also J.Bicak, V.Janis, *MNRAS* **212**, 899, (1985).
- [11] Lovelace R.V.E., *Nature* **262**, 649, (1976).
- [12] Lovelace R.V.E., MacAuslan J., Burns M.L., *AIP Conf. Proc.*, **56**, 399, (1979).
- [13] Blandford R.D., Znajek R.L., *MNRAS*, **179**, 433, (1977).
- [14] Beskin V.S., Istomin Ya.N., Par'ev V.I., *Soviet Astronomy*, **36**, 642, (1992).
- [15] A. Neronov, D. Semikoz, F. Aharonian and O. Kalashev, *Phys. Rev. Lett.*, **89**, 051101, (2002).
- [16] A. Y. Neronov and D. V. Semikoz, *New Astr. Rev.*, **47**, 693, (2003).
- [17] A. Y. Neronov and D. V. Semikoz, *Phys. Rev. D*, **66**, 123003, (2002).
- [18] Thorne K.S., Price R.H, Macdonald D.A., *Black holes: The membrane paradigm*, Yale University Press, (1986).
- [19] K. Greisen, "End To The Cosmic Ray Spectrum?," *Phys. Rev. Lett.*, **16**, 748, (1966);
- [20] G. T. Zatsepin and V. A. Kuzmin, "Upper limit of the spectrum of cosmic rays," *JETP Lett.*, **4**, 78, (1966) [*Pisma Zh. Eksp. Teor. Fiz.*, **4**, 114, (1966)].
- [21] R. Abbasi *et al.* [HiRes Collaboration], arXiv:astro-ph/0703099.
- [22] M. Roth [PAO Collaboration], "Measurement of the UHECR energy spectrum using data from the Surface Detector of the Pierre Auger Observatory," arXiv:0706.2096 [astro-ph]. See also

http://www.auger.org/technical_info/spectrum2007/spectrum_icrc07.html

- [23] M. Kachelriess and D. V. Semikoz, *Astropart. Phys.*, **26**, 10, (2006).
- [24] A. Cuoco, G. Miele and P. D. Serpico, *Phys. Rev. D*, **74**, 123008, (2006).
[arXiv:astro-ph/0610374].
- [25] Abraham J. et al.[PAO Collaboration] *Science* **318**, 939, (2007).
- [26] Berezhinsky, V. S.; Grigor'eva, S. I. *Proc. 15th International Cosmic Ray Conference*, (1977); Berezhinsky, V. S., Bulanov S. V., Dogiel, V. A., Ginzburg, V. L., & Ptuskin, V. S. 1990, *Astrophysics of Cosmic Rays* Elsevier (1990).
- [27] E. Boldt and P. Ghosh, *MNRAS*, **307**, 491, (1991).
- [28] Bardeen J.M., Petterson J.A., *Ap.J.* **195**, L65, (1975).
- [29] Bardeen, J.M., Press, W.H., Teukolsky, S.A., *Ap.J.* **178**, 347 (1972).
- [30] Goldreich P., Julian W.H., *Ap.J.* **157**, 869, (1969).
- [31] W.H.Press *et al.*, *Numerical Recipes in C: The Art of Scientific Computing*, Cambridge University Press, 1992. See also online edition <http://www.nr.com/>.
- [32] Landau L.D., Lifshitz E.M., *The Classical Theory of Fields*, Elsevier (1980).
- [33] B.Carter, *Phys.Rev.* **174**, 1559, (1968).
- [34] T. Erber, *Rev. Mod. Phys.*, **38**, 626, (1966).
- [35] D. Allard *et al.*, *JCAP* **0609** 005, (2006).
- [36] Genzel, R., et al. *MNRAS*, **317**, 348, (2000).
- [37] Bird D.J. et al. *Ap.J.* **424**, 491, (1994).
- [38] Aharonian F. et al., *A&A* **425**, L13, (2004).
- [39] R. Schodel *et al.*, *Nature*, **419**, 694, (2002).
- [40] N. Haring-Neumayer, M. Cappellari, H. W. Rix, M. Hartung, M. A. Prieto, K. Meisenheimer and R. Lenzen, *Ap. J.* **643**, 226, (2006).
- [41] M. Kachelriess, E. Parizot and D. V. Semikoz, arXiv:0711.3635 (2007).